

## A DERIVING Equation (5)

For a Brownian motion process as described by Equation (1),

$$\begin{aligned} A(0; v) &= 0, \\ A(t; v) &= vt + W(t) \\ W(t) &\sim \mathcal{G}(0, t), \end{aligned}$$

the joint probability distribution of an evidence value  $a$  observed at time  $t$  is described by the Fokker-Plank equation:

$$\frac{\partial p}{\partial t} + v \frac{\partial p}{\partial a} = \frac{1}{2} \frac{\partial^2 p}{\partial a^2}, \quad (14)$$

with boundary conditions

$$\begin{cases} p(0, a) = \delta(a) \\ p(t, \alpha) = 0 \end{cases} \quad (15)$$

where  $p$  is the probability density function of particles behaving according to Equation (1), and  $\delta$  is the Dirac delta function. The solution to the boundary value problem described by Equation (14), with boundary conditions of Equation (15), is

$$p(t, a) = \frac{1}{\sqrt{2\pi t}} \left( \exp \left[ -\frac{(a-vt)^2}{2t} \right] - \exp \left[ 2v\alpha - \frac{(a-2\alpha-vt)^2}{2t} \right] \right). \quad (16)$$

This probability density function describes the joint probability of observing any given pair of time  $t$  and evidence  $a$ . Using this density function, we first compute the probability of the evidence being below the threshold,  $\alpha$ . For the distribution of first passage time,  $T$ , this probability is equivalent to the survival function. I.e.,

$$S(t) = P(T > t) = \int_{-\infty}^{\alpha} p(t, a) da. \quad (17)$$

Plugging in Equation (16) into Equation (17) we get,

$$S(t) = \Phi \left( \frac{\alpha - vt}{\sqrt{t}} \right) - \exp(2v\alpha) \Phi \left( \frac{-\alpha - vt}{\sqrt{t}} \right). \quad (18)$$

Finally, we are able to derive the probability density function of  $T$  via the relation between the PDF function and the survival function:

$$\begin{aligned} h(t) &= -\frac{dS}{dt} \\ &= \frac{\alpha}{\sqrt{2\pi t^3}} \exp \frac{-(\alpha - vt)^2}{2t}. \end{aligned} \quad (19)$$

## B DATA NORMALIZATION PSEUDO-CODE

We describe the normalization and calibration procedures applied that are necessary for optimizing and subsequently using the model for novel applications.

**Require:** pilot study data

- 1: pick a pedestal condition (e.g.  $c = 1.0, f = 1.0, e = 0^\circ$ )
- 2: **for** each subject **do**
- 3:   compute the average latency of pedestal condition,  $t_{\text{pedestal}}$
- 4:   scale **all** latencies by  $1/t_{\text{pedestal}}$
- 5: **end for**
- 6: train RBF network for computing  $v$  in normalized units
- 7: **return** normalized  $v$  predictor.

Algorithm 1. Normalization.

Once we obtain an optimized  $v$  predictor, we apply the model to a novel application as follows:

**Require:** target application sample data

- 1: measure the  $\mathbb{E}$  and  $\mathbb{V}$  of the latency
- 2: compute  $\alpha$  for data using eq. (7)
- 3: rescale  $v$  by  $\mathbb{E}$  of the data
- 4: **return** probability distribution described by  $\alpha$  and rescaled  $v$ .

Algorithm 2. Calibration.

Due to the inverse correlation between the step 4 in Alg. 1 and the step 3 in Alg. 2, any selection of condition in step 1 of Alg. 1 does not lose the generality.

## C DERIVING Equation (13)

We are interested in deriving an expression for the probability distribution function for  $T_{dual}$  as shown in Equation (12).

$$T_{dual} = \max(T_f, T_p).$$

We know that both  $T_f$  and  $T_p$  are Inverse Gaussian (IG) random variables as detailed in Equation (10),

$$\begin{aligned} T_f &\sim \mathcal{IG}(\alpha_f, v_f) \\ T_p &\sim \mathcal{IG}(\alpha_p, v_p). \end{aligned}$$

The probability that  $T_{dual}$  is less than some time  $t$  is equivalent to the statement that both  $T_f$  and  $T_p$  are less than  $t$ . I.e.,

$$P(T_{dual} \leq t) = P(T_f \leq t)P(T_p \leq t), \quad (20)$$

or,

$$H_{dual}(t) = H_f(t)H_p(t), \quad (21)$$

where  $H_f$  denotes the cumulative density function (CDF) of the IG distribution with parameters  $\alpha_f$  and  $v_f$ , and vice versa for  $H_p$ . The probability density function of  $T_{dual}$  is therefore equal to the derivative of  $H_{dual}$ .

Taking the derivative from Equation (21) we get,

$$h_{dual}(t) = h_f(t)H_p(t) + H_f(t)h_p(t). \quad (22)$$

Since we have an explicit expression for the PDF of  $T_{dual}$ , we can finally write down an expression for the likelihood function from Equation (13) as

$$\begin{aligned} L(\alpha_f, \alpha_p; t, v_f, v_p) &= h(t; \alpha_f, v_f)H(t; \alpha_p, v_p) + \\ &\quad + H(t; \alpha_f, v_f)h(t; \alpha_p, v_p), \end{aligned} \quad (23)$$

where  $h$  and  $H$  are the PDF, and CDF functions of the IG distribution.

## D FIELD-OF-VIEW VS ECCENTRICITY & FREQUENCY

The observed image characteristics of stimuli shown on a display vary depending on how far the display is from the eye. We correlate these effects using the field-of-view that the display occupies as a measure of eye-distance. FoV is an intuitive way to measure eye-distance as it can be used regardless of the specific dimensions of a given display.

Given a display with width  $w$ , presented at an FoV of  $\theta_{\text{fov}}$ , the distance of the display equals

$$d = \frac{w/2}{\tan(\theta_{\text{fov}}/2)}. \quad (24)$$

If an observer is staring at the center of the display at FoV of  $\theta_{\text{fov}}$  (or equivalently at a distance of  $d$ ), an object  $x$ cm away from the center of the display will appear at

$$\theta = \arctan \frac{x}{d} = \arctan \left( x \frac{\tan(\theta_{\text{fov}}/2)}{w/2} \right) \quad (25)$$

retinal eccentricity. Hence, we notice that changing the eye-distance of a display alters the eccentricity at which stimuli appear in the retina.

Additionally, we can use this relation to derive a rate-of-change coefficient between physical distances (in cm), and retinal eccentricities (in degrees) by taking the derivative of eq. (25),

$$\frac{d\theta}{dx} = \frac{\cos^2 \theta}{d} = \cos^2 \theta \frac{\tan(\theta_{\text{fov}}/2)}{w/2}. \quad (26)$$

This measure of “degrees-per-distance” allows us to derive the relationship between the spatial frequency of a pattern shown on the screen,  $f_{\text{display}}$  (in cycles-per-centimeter), and the retinal frequency that an observer perceives,  $f_{\text{retina}}$  (in cycles-per-degrees),

$$f_{\text{retina}} = f_{\text{display}} \frac{1}{\cos^2 \theta} \frac{w/2}{\tan(\theta_{\text{fov}}/2)}. \quad (27)$$

Note that the observed frequency not only depends on the FoV, but also the eccentricity at which the stimulus is shown. For the simplest case where the stimulus is at the center of the screen, or  $\theta = 0$ , the relationship simplifies to

$$f_{\text{retina}} = f_{\text{display}} \frac{w/2}{\tan(\theta_{\text{fov}}/2)}. \quad (28)$$

## E PLOTS FOR INDIVIDUAL PARTICIPANTS IN PRELIMINARY STUDY (Section 3)

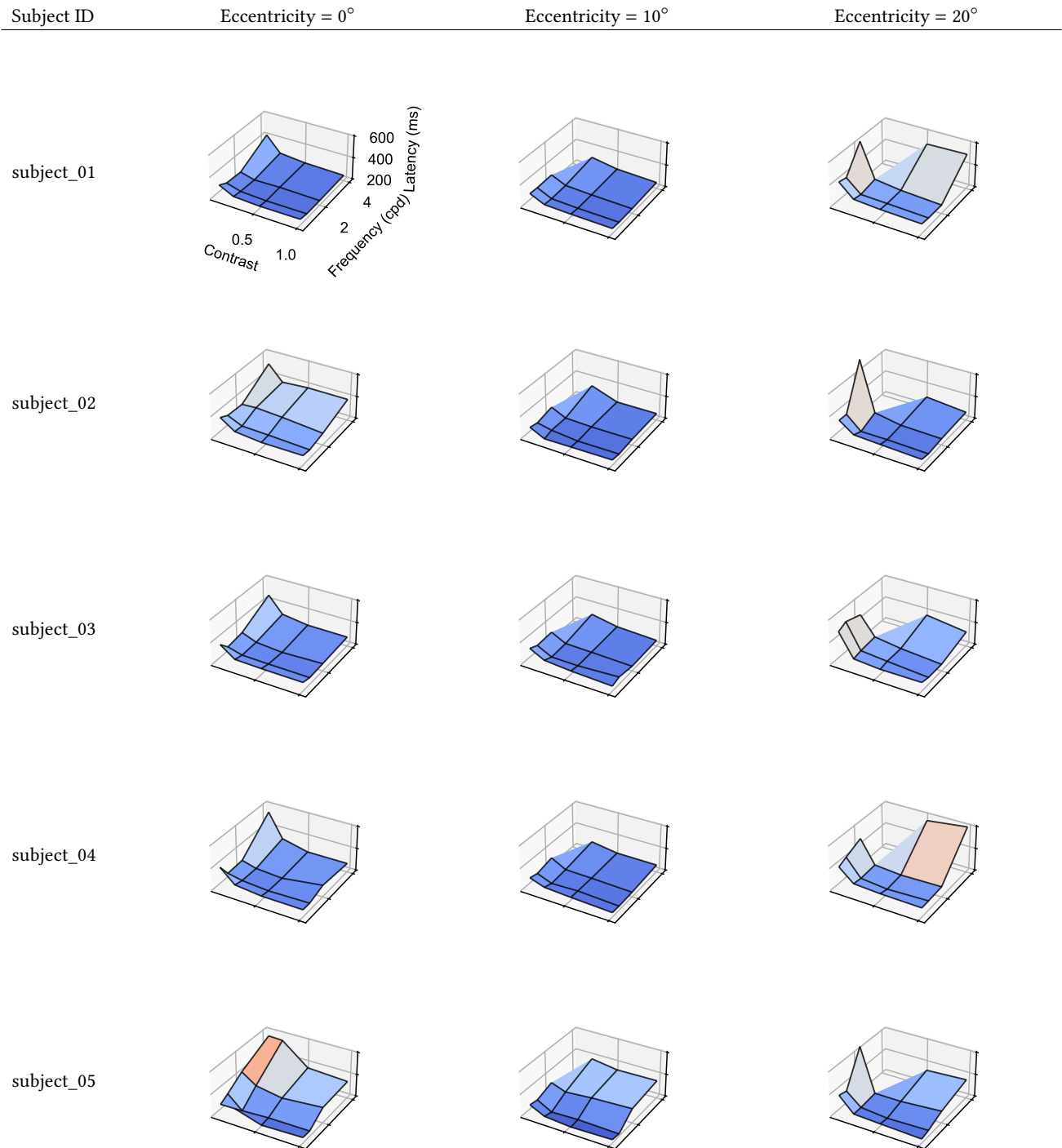


Fig. 10. Aggregated data of the pilot experiment. Each subject completed 50 repetitions for each of the 45 conditions across 10 blocks of the user study. Each vertex in these surfaces represent the mean saccade latency of 50 trials with the same condition for each subject.

## F PLOTS FOR ABLATION STUDY CONDITIONS (Section 6.1)

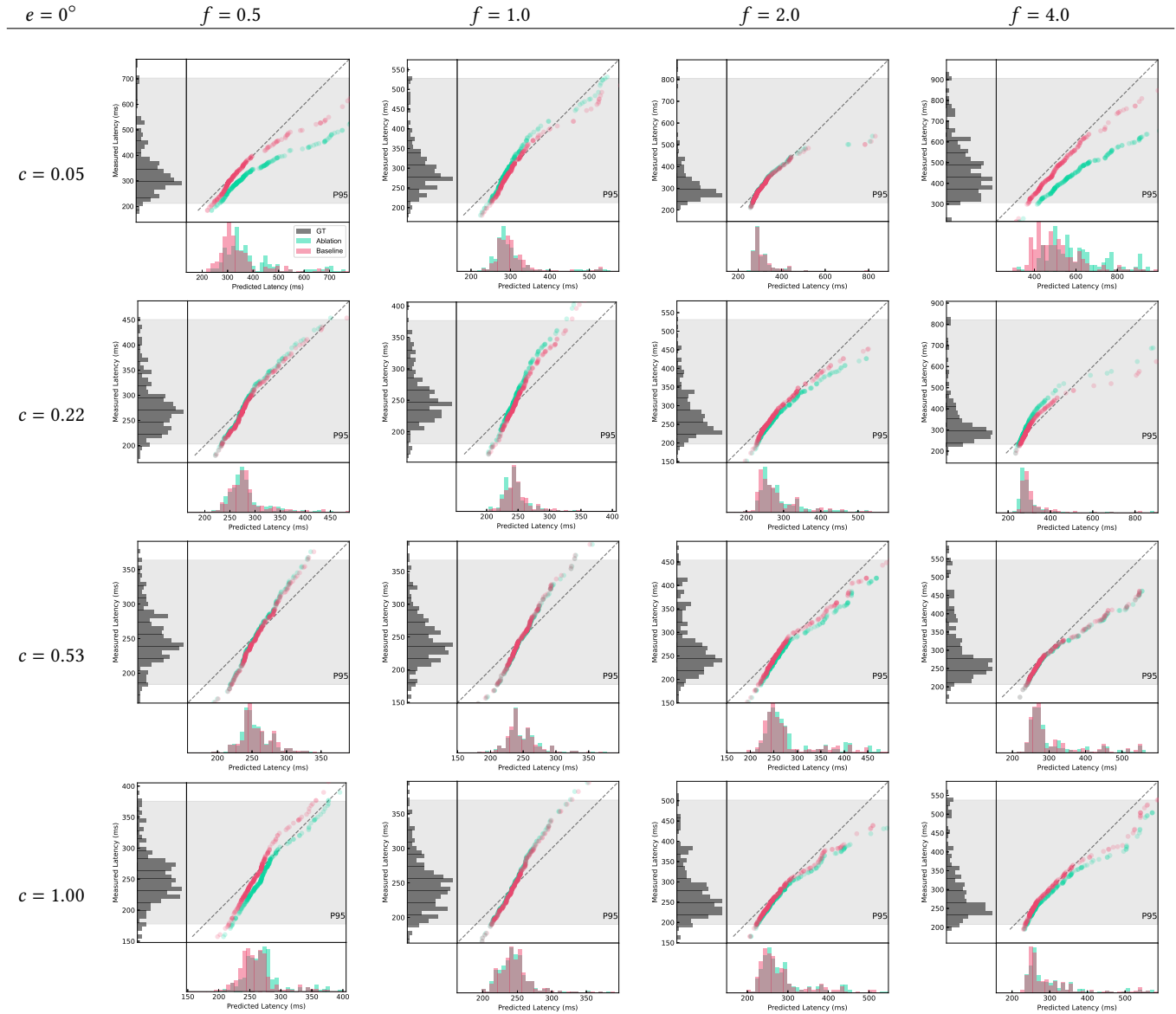


Fig. 11. Ablation study plots when any single condition is removed (as described in Section 6.1) from the training dataset where eccentricity  $e = 0^\circ$ . By observing the corresponding model performance drop (i.e., stronger misalignment with the  $y = x$  line), we visualize individual visual characteristic condition's contribution to the model. We observe that the distribution of latencies for some conditions cause a larger regression in the model's performance, such as the conditions  $(c = 0.05, f = 0.5, e = 0^\circ)$  and  $(c = 0.05, f = 4.0, e = 0^\circ)$ . These regressions are caused by the fact that the model strongly relies on the data we collected for these specific conditions. Meanwhile, when conditions, such as  $(c = 0.53, f = 1.0, e = 0^\circ)$ , are removed for ablation the model is able to successfully interpolate their predictions, due to the abundance of neighbor conditions. To quantify the sizes of the regressions, we compute the MSE of ablated models against the ground truth data, and compare how much the error increased/decreased when compared to the full model. On average, the MSE of the ablated model regresses by as much as 50% when compared to the full model. However, the regression in performance is largely attributed by a few conditions which we mentioned above with the condition  $(c = 0.05, f = 4.0, e = 0^\circ)$  exhibiting a 1100% increase in error. If we discount the extreme conditions, we observe that the median MSE regression is equal to 7%.

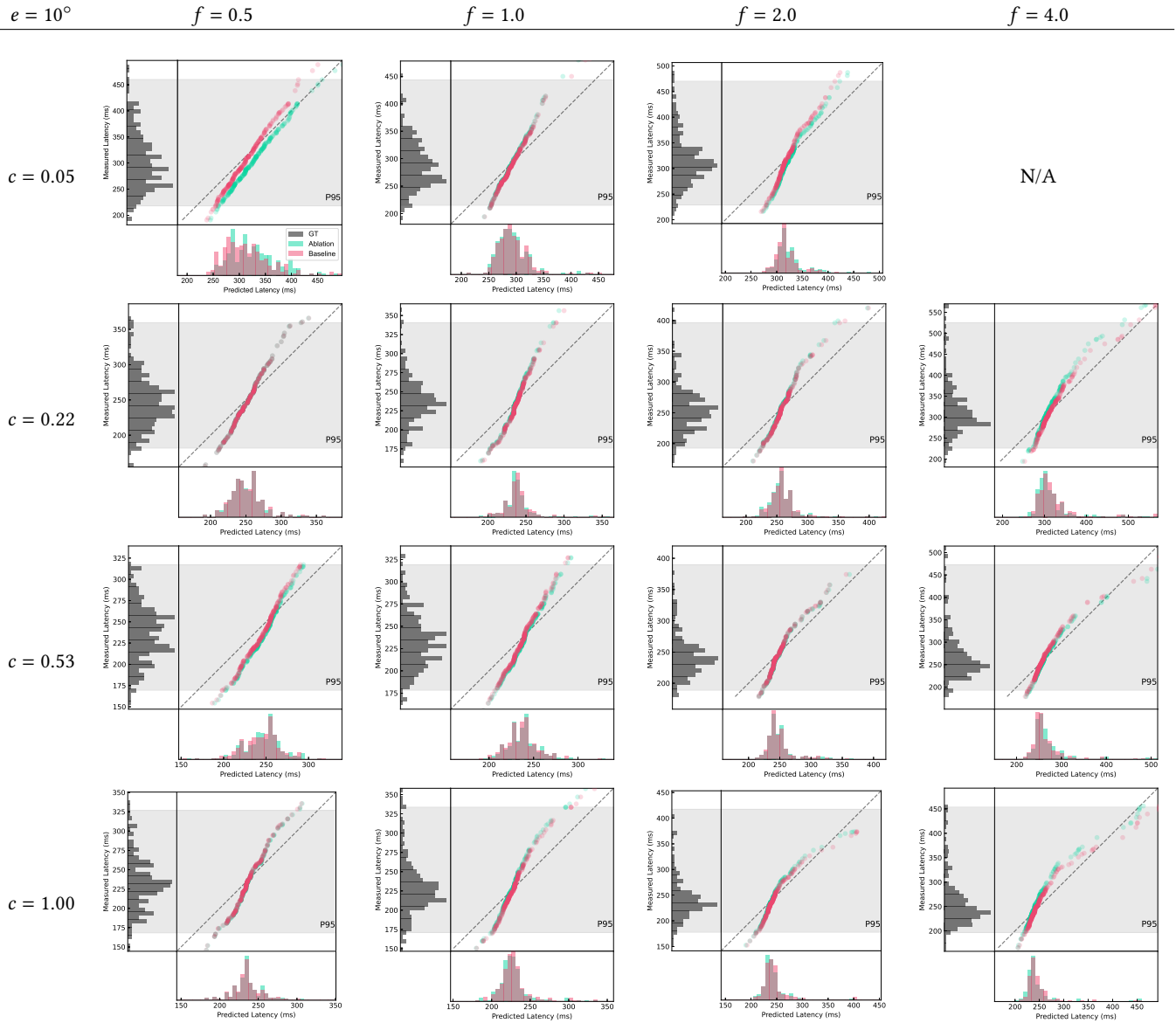


Fig. 12. Ablation study plots when any single condition is removed (as described in Section 6.1) from the training dataset where eccentricity  $e = 10^\circ$ . See Figure 11, for further analysis.

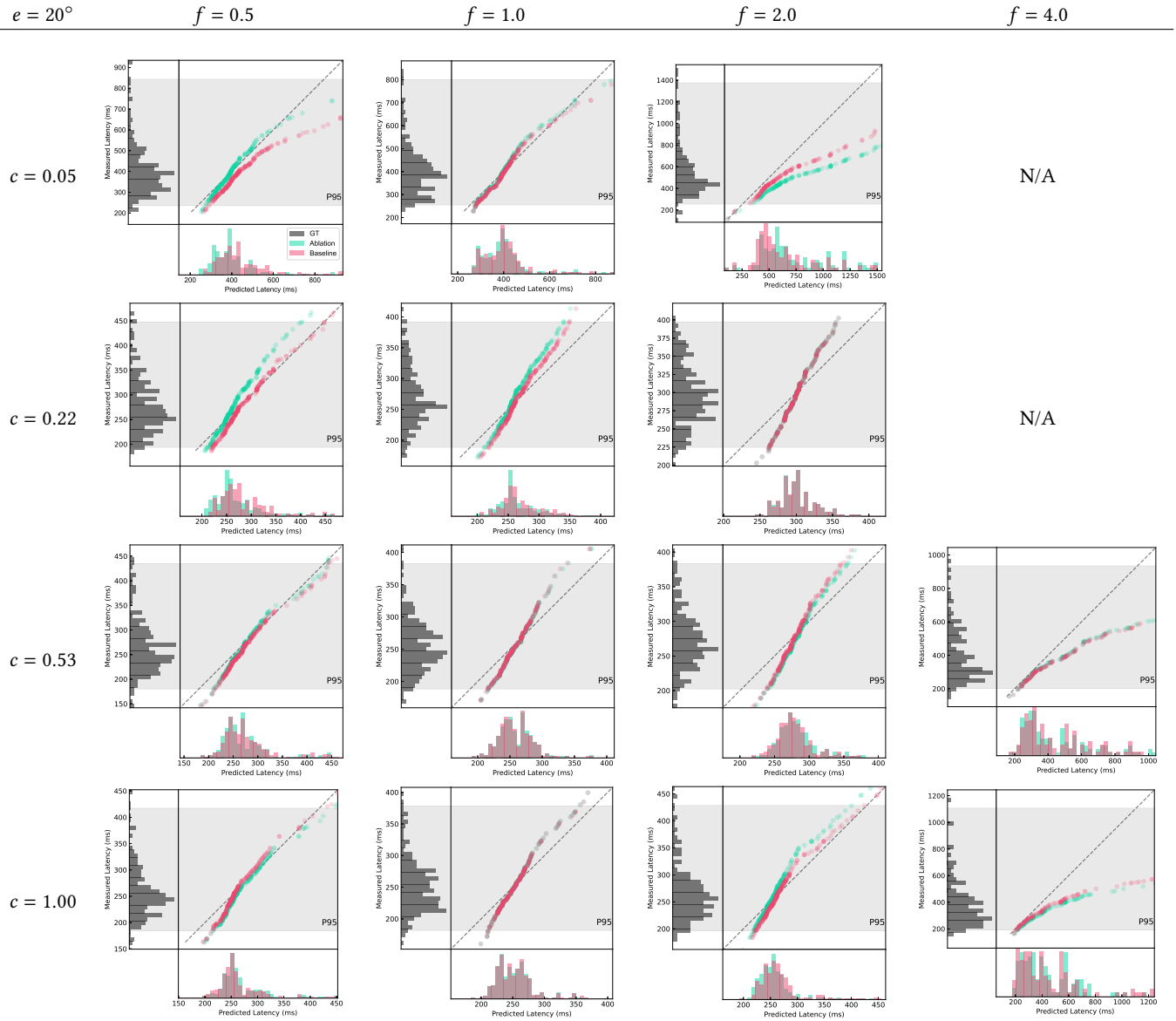


Fig. 13. Ablation study plots when any single condition is removed (as described in Section 6.1) from the training dataset where eccentricity  $e = 20^\circ$ . See Figure 11, for further analysis.

## G PLOTS FOR INDIVIDUAL PARTICIPANTS IN NATURAL TASKS (Section 6.2)

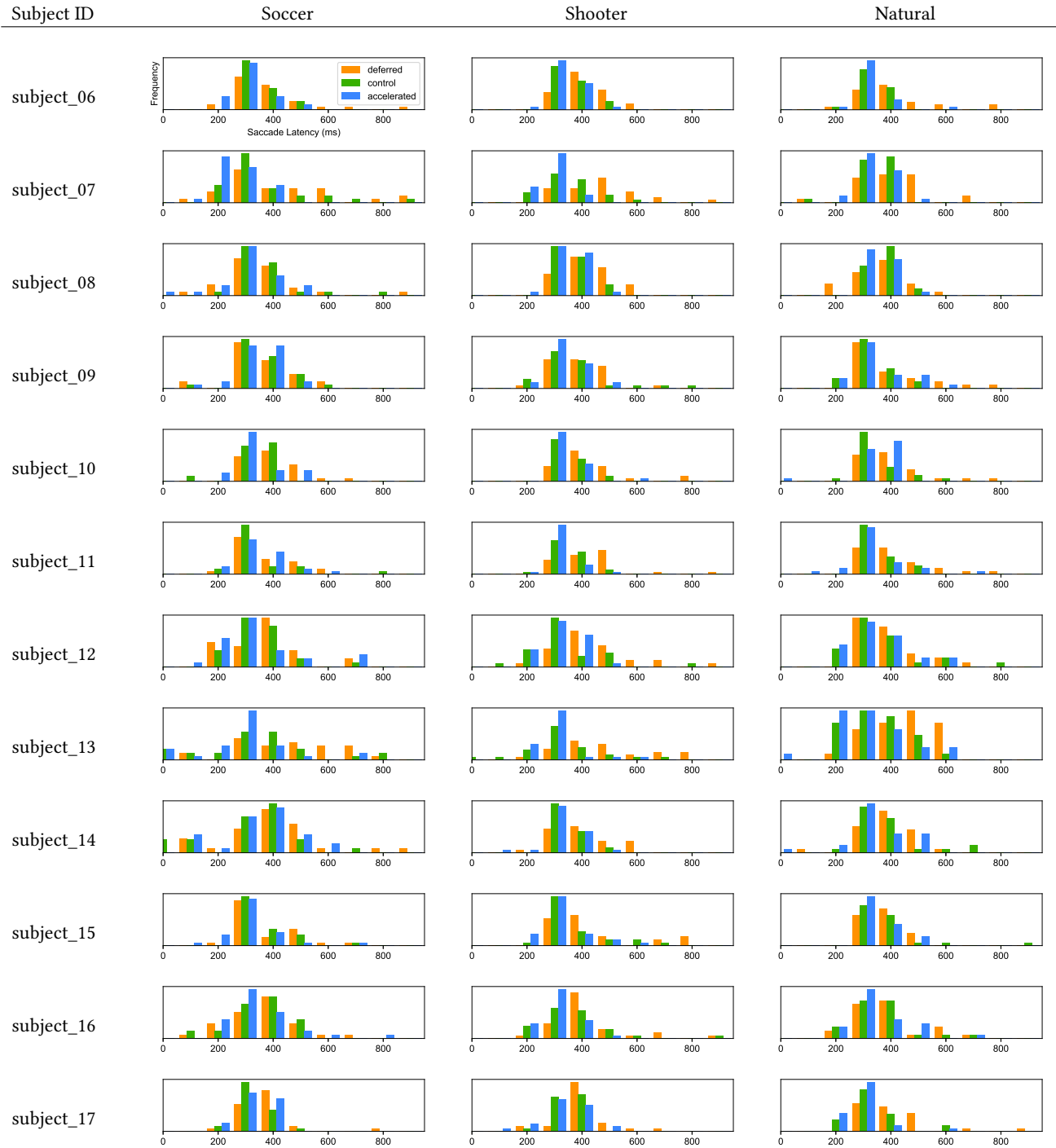


Fig. 14. Saccade latency histograms for Figure 7. Each subject completed 51 trials for each condition, for each scene for a total of 459 trials. The latencies have been normalized to a common mean to enable quick comparisons between histograms.